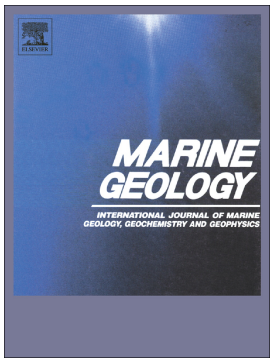

Structural controls on slope evolution and sediment dispersal pathways along the northern Tanzania continental margin, western Indian Ocean

Marina Dottore Stagna, Vittorio Maselli, Djordje Grujic, Pamela Reynolds, David Reynolds, David Iacopini, Bill Richards, John R. Underhill, Dick Kroon

PII: S0025-3227(21)00244-9

DOI: https://doi.org/10.1016/j.margeo.2021.106662

Reference: MARGO 106662

To appear in: *Marine Geology*

Received date: 19 March 2021

Revised date: 10 September 2021

Accepted date: 2 October 2021

Please cite this article as: M.D. Stagna, V. Maselli, D. Grujic, et al., Structural controls on slope evolution and sediment dispersal pathways along the northern Tanzania continental margin, western Indian Ocean, *Marine Geology* (2021), https://doi.org/10.1016/j.margeo.2021.106662

Title: Structural controls on slope evolution and sediment dispersal pathways along the northern Tanzania continental margin, western Indian Ocean.

Authors: Marina Dottore Stagna[1], Vittorio Maselli[1], Djordje Grujic[1], Pamela Reynolds[1], David Reynolds[1], David Iacopini[2], Bill Richards[1], John R. Underhill[3], Dick Kroon[4]

Affiliations:

[1] Department of Earth and Environmental Sciences, Dalhousie University, Halifax, Nova Scotia, Canada

[2] Dipartimento di Scienze della Terra, dell'Ambiente e delle Risorse, University of Naples "Federico II", Naples, Italy

[3] Centre for Exploration Geoscience, Applied Geoscience Unit, Institute of GeoEnergy Engineering (IGE), School of Energy, Geoscience, Infrastructure & Society, Heriot-Watt University, Edinburgh, United Kingdom

[4] School of GeoSciences, University of Edinburgh, Edinburgh, United Kingdom

Highlights

- This study provides new constraints on the evolution of the North Tanzanian margin.
- Changes in canyon-channel systems were reconstructed from Oligocene to recent times.
- Uplift of Pemba and Zanzibar islands controlled the evolution of slope systems.
- Pemba and Zanzibar formed during mid-upper Miocene and Mio-Pliocene, respectively.
- Extensional regime associated with islands' emersion may be related with the EARS.

ABSTRACT

In this study, we investigate the tectonic and stratigraphic evolution of the northern Tanzania margin (western Indian Ocean) to provide new insights on the structural drivers governing the

formation of Zanzibar and Pemba islands. Using 2D seismic reflection profiles and exploration wells, we have reconstructed the evolution of the submarine drainage network throughout the last 30 Myr, from the Oligocene to recent times, providing a tape-recorder with which we determine the different tectonic events that led to the eventual subaerial exposure of the islands. In detail, we observe a decrease in the number of slope canyon-channel systems during the lower-middle Miocene offshore Pemba Island that we interpret to represent the initial uplift of the island: tectonic deformation of the seafloor impeded up-dip to down-dip sediment transfer, forcing the abandonment of canyon-channel systems. At the same time, submarine canyons were still active offshore Zanzibar Island, located ~35 km south of Pemba, indicating that its uplift occurred later, likely during the upper Miocene to lower Pliocene. The uplift of the islands increased the slope gradient and promoted the formation of two newly discovered giant canyons that represent the main feeder systems to this sector of the western Indian Ocean since the Miocene. We propose a new conceptual model for the post-Oligocene evolution of the area, highlighting the main tectonic structures and their timing of formation. In this model, the onset of the anticlines of Pemba and Zanzibar islands resulted from tectonic inversion probably originated during the Oligocene-lower Miocene due to reactivation of Mesozoic-aged rift faults. This compressional phase is followed by the establishment of an extensional tectonic regime which promoted the subaerial exposure of the islands since the middle Miocene. Extensional faults, which dissect the post-Oligocene stratigraphy, create horsts and grabens on a variety of scales, such as Zanzibar and Pemba troughs. These grabens show comparative size and orientation to onshore rift basins, which may indicate a relation with the tectonics of the East African Rift System. Our results provide new insights on the evolution of one the least explored, though fascinating, continental margin settings worldwide that can support future source-to-sink investigations in the region.

KEYWORDS: Tanzania margin; Pemba and Zanzibar islands, East African Rift System; Indian Ocean; Submarine canyons; Tectonics.

1. INTRODUCTION

The outer shelf and upper slope regions of the East Africa continental margin offshore northern Tanzania (western Indian Ocean) are dissected by the anticline of Pemba and Zanzibar islands (Fig. 1). The presence of these structures suggests that the evolution of the margin is more complex than an idealized passive margin model (Sii and Underhill, 2015), which does not otherwise justify the presence of shelf and upper slope sediments uplifted above sea level. In recent years, the existence of an offshore branch of the East African Rift System (EARS) in the western Indian Ocean has been proposed to explain the formation of submarine grabens and related uplifted regions with similar orientation and geometry of onshore rifts, such as the Kerimbas Graben and Davie Ridge (Mougenot et al., 1986; Franke et al., 2015; Klimke and Franke, 2016; Maselli et al., 2019). However, as of today, only a few studies have focused on the origin of Pemba and Zanzibar islands and related troughs, with Stockley (1942) first postulating a separation of these islands from Africa during the upper Miocene and a relation with the EARS tectonics. Yet, many questions about the origin of the islands, the precise timing of their formation, and the relation with the EARS tectonics remain unanswered. Furthermore, a quantification of the effects of tectonic seafloor deformation on the evolution of the slope depositional system is still lacking. These knowledge gaps prevent a thorough understanding of the evolution of the Tanzania margin, with implications for source-to-sink sediment transfer in the western Indian Ocean.

In this study, we analyze 2D seismic reflection profiles and exploration wells to investigate the Oligocene to Recent stratigraphy of the northern Tanzania margin offshore Zanzibar and Pemba islands, from the outer shelf to about 3000 m of water depth. Our goal is to understand how slope canyon-channel systems are progressively disconnected from their feeding systems and abandoned as a result of the basin floor uplift. By dating changes in the submarine drainage network and sediment fluxes, together with a quantification of the timing of fault activity, we aim to provide a detailed chronology for the structural and stratigraphic evolution of the margin over the last 30

million years and explore the formation of the islands and how they relate to the tectonics of the EARS.

2. GEOLOGICAL SETTING

The break-up of Gondwana started in the lower Jurassic and led to the formation of the rifted margins of East Africa and Madagascar during the upper Cretaceous and lower Cenozoic (Heirtzler and Burroughs, 1971; Mougenot et al., 1986). Sediment deposition along the conjugate margins occurred during a tectonically quiescent period that was interrupted during the Eocene by the formation of a new mantle plume impinging on the base of the thick cratonic African lithosphere, which led to the initiation of the East African Rift System (EARS; Burke, 1996; Ebinger et al., 1998; Buitner, 2014). In Tanzania, the EARS has developed in two branches, which formed synchronously during the upper Oligocene - lower Miocene (Roberts et al., 2012). Normal faulting has occurred along both the Western and Eastern branches of the rift, which are currently separating at a rate of 4 mm yr^{-1} and 2 mm yr^{-1} in the northern and southern parts, respectively (Calais et al., 2006). Regional doming and rift flank uplift have had a profound effect on the development of modern drainage systems as well as regional climate, thus directly influencing sediment supply to the western Indian Ocean (Semuche et al., 2006, Maselli et al., 2020).

The Tanzania margin presents a few-km-wide shelf in the Rovuma delta region, where the slope is dissected by the Kerimbas Graben and Davie Ridge, and an up to ~70-km-wide shelf where the Rufiji and Ruvu river deltas develop (Anthony et al., 2021). The width of the shelf reduces to few kilometers north of 5°30’ S, where almost a kilometer-deep basin separates the mainland from Pemba Island (Fig. 1). The complex Meso-Cenozoic geological history, combined with the lack of detailed chronological constraints, has made understanding of these structures difficult. The Kerimbas Graben and Davie Ridge, which are part of the Davie Fracture Zone (DFZ), deform the slope in water depths greater than 1000 m. The DFZ was initially interpreted as the transform fault system associated with the southward drift of Madagascar and extending between 20°S and 2.5°S

latitude (Mougenot et al., 1986; Reeves, 2000; Reeves, 2018 and references therein). Recent studies, however, have proposed an alternative model for the formation of the DFZ and the uplift of the Davie Ridge, thus, implying a different pre-rift paleo-position of Madagascar with respect to Africa (Franke et al., 2015; Klimke and Franke, 2016; Vormann and Jokat, 2021). In this model, Madagascar was located adjacent to present-day offshore Tanzania-Mozambique, and only the southernmost portion of the DFZ, south of 10° S, was related to a strike-slip fault oriented roughly parallel to the eastern coast of Africa. Consequently, the origin of the Kerimbas Graben and the Davie Ridge has been related to transtensional forces due to the development of an offshore branch of the EARS since the Oligo-Miocene (Franke et al., 2015; Klimke and Franke, 2016). The discovery of abandoned deep-water channels of Neogene age along the crest of the Davie Ridge has corroborated this new model (Maselli et al., 2019).

Zanzibar Island has a surface area of 1464 km^2 and has a maximum topographic elevation of ~120 m, while Pemba covers 988 km^2 and has a maximum topographic elevation of ~90 m. The surficial geology of Zanzibar Island is characterized by Miocene sandstones, shales, and reef limestones (Kent et al., 1971), while Pemba Island consists of Miocene shales and sandstones (Chake Chake and Weti beds), and Pleistocene reef limestones (Kent et al., 1971). Topography, surface geology, and gravimetric data show that the islands represent anticlinal folds and tilted fault blocks (Kent et al., 1971; Sii and Underhill, 2015), which structural axis is broadly oriented SSW-NNE and S-N for Pemba and Zanzibar Island, respectively (Kent et al., 1971).

2.1. Pemba and Zanzibar islands: previous interpretations and models

One of the first reports on the evolution of the islands dates to the first half of the XX century, when von Staff (1914) proposed that Pemba Island formed during the Pleistocene in response to the tectonic activity of the East African rift. This hypothesis was refuted by Stockley (1928; 1942) based on the timing of the transition between the fossiliferous Miocene Chake Chake beds and the non-fossiliferous fluvial and estuarine Weti beds. The author counter-proposed that Pemba has not

been connected with Africa at least since the Miocene, while Zanzibar Island only since Pleistocene times.

By analyzing new paleontological evidence from fossil fauna and flora, Moreau and Pakenham (1940; 1941) concluded that the trough that separates Pemba Island from the continent resulted from the Pleistocene activity of the East African rift, in agreement with von Staff (1914).

Later, Kent et al. (1971) analyzed gravimetric and seismic data in combination with three exploration wells (including Zanzibar-1 and Pemba-5, Figs.1A and 2A) and reconstructed an Oligocene-Miocene rock uplift of ~200 m based on subsidence curves. The authors proposed that Pemba and Zanzibar islands were already taking shape during the upper Oligocene and Miocene due to deformation associated with NNW-SSE and NE-SW striking normal faults, and that the Pemba trough formed in the Pliocene as an asymmetric graben. The islands' development was related to several deformational pulses that the authors tentatively dated as upper Miocene, upper Pliocene, and a minor pulse in the lower Pleistocene (Kent et al., 1971), also suggesting a relation with the EARS considering the similarity of the Pemba-Zanzibar troughs with the onshore rift valleys.

Terrestrial mammals with affinities of African continental faunas were discovered in middle Miocene deposits on Pemba Island, thus revealing that the island was inhabited by taxa that occurred on the African mainland at ca. 16.5 million years ago (Pickford, 2008).

More recently, Sii and Underhill (2015) presented a deep seismic profile across the islands (see line drawing in Figure 1C) and used onshore (Zanzibar-1 and Pemba-5) and offshore (Simba-1) exploration wells to derive the broad chronology of post-Cretaceous seismic horizons (Figs. 1B, C, and 2). The authors proposed that the folds leading to the formation of the islands resulted from long-lived and punctuated tectonic inversion of pre-existing normal faults, and that a lower Oligocene to upper Miocene timing for this contractional deformation is coeval with the EARS tectonics. The authors assumed that the DFZ acted as a buttress controlling the change in stress and

inducing uplift of the islands, and they proposed that the roughly E-W compression is still ongoing while the faults still appear in net extension (Sii and Underhill, 2015).

However, more recent studies conducted on gravimetric and seismic reflection data concluded that there is no evidence for the continuation of the DFZ offshore northern Tanzania and Kenya (Franke et al., 2015; Klimke and Franke, 2016; Sauter et al., 2018; Vormann and Jokat, 2021). Sauter et al. (2018) demonstrated that gravity anomalies previously interpreted as an expression of the DFZ are related with a compressional phase between the Hautervian and Aptian (~132 to 120 Ma) that produced reverse fault structures localized in deep-water and affecting the Jurassic to lower Cretaceous units. Furthermore, the moment tensors of offshore earthquakes recorded in the last 40 years (Yang and Chen, 2010), including the M 6.0 event that occurred near the coast of Dar es Salaam on 12 August 2020 (Fig. 1A), indicate that the area is roughly in W-E extension.

Davidson and Steel (2018) associated the formation of the Zanzibar and Pemba trough to the transtensional strike-slip movement along N-S-trending faults, which are still active today, and concluded that the two islands are basement-cored Neogene highs caused by inversion.

3. MATERIALS AND METHODS

3.1. 2D Seismic reflection data

This study is based on a set of 5550 km of 2D multichannel seismic reflection profiles from the Tanzania 1999/2000 Multiclient 2D survey, which was acquired by WesternGeco-Schlumberger using a 5200-m-long streamer with hydrophones at a 12.5 m receiver interval. Due to the commercial potential of the area for hydrocarbon exploration, these 2D seismic profiles are truncated ca. 100 ms below the Oligocene interval (M2 horizon). The seismic data were reprocessed in 2012 introducing an anisotropic Kirchhoff pre-stack time migration. The vertical resolution between the seafloor and horizon M2 is from 6.25 m to 9.2 m, calculated considering a peak frequency of 60 Hz and interval velocity of 1500 to 2200 m s^{-1}, as derived from checkshot data of Well-1 (Fig. 1, see also Maselli et al., 2020).

We integrated this dataset with the 2D multichannel seismic reflection profiles acquired by Lamont-Doherty Geological Observatory during the expedition V3618 (Rabinowitz, 2005), conducted in 1980 on board of the R/V Vema. These multichannel seismic data were acquired using a 1200-m-long streamer with 12 channels and recorded at 4 ms intervals by using a Texas Instruments DFS IV digital acquisition system (Rabinowitz, 2005). We also made use of the post-stack depth-migrated (PSDM) 2D seismic profile presented by Sii et al. (2015), for which a line-drawing is shown in Figure 1C.

The terminology used for the description of the variation in acoustic impedance is according to Veeken et al. (2013): we utilize the term "hard kick" to indicate a downwards increase in acoustic impedance while "soft kick" denotes a downward decrease in acoustic impedance.

3.2. Well data

Data from five exploration wells were used in this study (Figs. 1, 2). All the offshore wells are crossed by at least one seismic profile (Fig. 1A, B).

The southernmost well used in this study, renamed *Well-1* for confidentiality, was drilled in 2014 in a water depth of 1375 m (Figs. 1A, 1B, and 2). Gamma-Ray (GR) data are available at a true vertical depth below mean sea level (ssTVD) between 1449 and 2442 m, while biostratigraphic data are available only below 2000 m ssTVD (Maselli et al., 2020).

Zanzibar-1 is located on Zanzibar Island at 35 m of elevation (Fig. 1A and 1B) and was drilled by the British Petroleum Company (BP) in 1957. The well penetrates Quaternary to Mesozoic sediments, reaching the upper Cretaceous at a depth of 4355 m (Fig. 2; Kent et al., 1971).

Pemba-5 was also drilled by BP in 1962 on the western side of Pemba Island at 25 m of elevation (Figs. 1A and 1B). The youngest sediments encountered in the well near the topographic surface are the Miocene 'Weti beds', while the oldest are upper Cretaceous at a depth of about 3886 m (Fig. 2; Kent et al., 1971).

Simba-1 is located offshore Kenya in water depths of 921 m. The well was drilled by Total in 1978 and reaches a depth of 3604 m below the seafloor, recovering upper Quaternary to Cretaceous sediments (Nyagah, 1994). The lithology and chronology of the Zanzibar-1 and Pemba-5 wells were reported by Kent et al. (1971), while Nyagah (1994) reported those of Semba-1.

The *Deep Sea Drilling Project (DSDP) Site 241*, the northernmost well, was drilled in 1972 offshore Kenya in water depth of 4054 m and reached upper Cretaceous sediments at a depth of 1174 m below the seafloor (Schlich et al., 1974).

3.3. Methodology

Seismic and well data were interpreted using Petrel software by Schlumberger. We applied conventional methods of Mitchum et al. (1977) to the seismic stratigraphic interpretation, whereby we sought to identify sequence boundaries marked by reflector terminations, through-going horizons, and subdivide the succession using seismic facies analysis. Five main horizons were identified and mapped throughout the data, namely M2, M2a, M3, M3a, and M4, from the oldest to the youngest, plus the seafloor reflection (water bottom). Horizons M2, M3, and M4 are the same as those defined by Maselli et al. (2020).

The chronology of each horizon was estimated through well ties (Fig. 2A). Horizon M2 ties Well-1 at 2129 m ssTVD and it is dated to 28 Ma (Rupelian to Chattian; Maselli et al., 2020). In DSDP Site 241, M2 correlates with the Eo-Oligocene unconformity at ~4518 m ssTVD (Blow, 1969; Schlich et al., 1974). M2 also corresponds to the Oligocene Unconformity of Sansom (2017, 2018).

Horizon M3 ties with Well-1 at 1655 m ssTVD and it is dated to 15 Ma (middle Miocene; Maselli et al., 2020). M3 intersects DSDP Site 241 at a depth of ~4434 m ssTVD, where middle Miocene sediments are encountered (Blow 1969). M3 can be correlated with the Near Top Miocene horizon (NTM) of Sii et al. (2015).

Horizon M4 ties Well-1 at 1475 m ssTVD and it is dated 5.3 Ma (base Pliocene; Maselli et al., 2020). M4 has been correlated with DSDP Site 241 at a depth of ~4202 m ssTVD, where lower Pliocene sediments are encountered (Blow, 1969).

Horizons M2a and M3a encounter Well-1 at a depth of ~1987 m ssTVD and ~1540 m ssTVD, respectively. Because biostratigraphic data are not available at these depths, the age of horizon M2a can be broadly defined considering the sediment accumulation rate in the interval between M2 and M3 horizons, which is 28.8 m/Myr (Maselli et al., 2020), and the distance of M2a to M2, which is ~142 m. Using this approach, the age of M2a is approximatively 23 Ma. Similarly, the age of horizon M3a can be broadly derived considering the sediment accumulation rate in the interval between M3 and M4 horizons, which is 18.6 m/Myr (Maselli et al., 2020), and the distance of M3a respect to M3, which is ~65 m. The age of M3a is, consequently, about 11.5 Ma. Physical correlation of horizons M2a and M3a with DSDP Site 241 was not possible, however their depth in the well was obtained using their chronology and is equal to ~4509 m and ~4334 m ssTVD, respectively. The depths of the horizons in DSDP Site 241 have been used to obtain the porosity of the units, as explained in the next section.

The five horizons plus the seafloor define five seismic units named U1, U2, U3, U4, and U5 that were characterized using five seismic facies (Figs. 3, 4, 5). The interpretation also included the identification of main erosional features, such as submarine canyons, based on reflection truncations, geometry, and seismic facies of the infill. Time-to-depth conversion of horizon maps was performed using a range of velocities from 1500 to 2200 m/s (Fig. 2B).

The volume of accumulated sediment was calculated for each of the five units using depth converted surfaces (Table 1). Volume values were also corrected for sediment compaction using Equation 1 (Steckler and Watts, 1978; Angevine et al., 1990):

$$V_S = V_B + V_B(\varphi_S - \varphi_B) \quad (1)$$

where V_S is the volume corrected for the compaction, V_B is the volume at a given depth, φ_S is the porosity at surface and φ_B is the porosity at a given depth. Porosity values used in this work are

from the well DSDP Site 241 (Deep Sea Drilling Project, 1989), which were fitted with an exponential curve of the form of Equation 2 from Athy (1930a) to account for the compaction of sediments (Table 1):

$$\varphi_B = 71.754\, e^{-0.001*z} \quad (2)$$

In the Equation 2, z is the depth in meters from the seafloor. The value of porosity at the surface is comparable with value in DSDP drill holes in the Indian Ocean (Métivier et al., 1999).

Sediment fluxes in 10^3 km^3/Myr and sedimentation rates in m/Myr were quantified for both the compacted (V_B; Table 1 and Fig. 2B) and decompacted volumes (V_S; Table 1) of each unit considering an area of ~37100 km^2. We evaluated the error in sediment flux calculations to be ±200 km^3 considering the vertical resolution of the seismic and a 20% of uncertainty in the porosity values as discussed by Métivier et al. (1999).

The reconstruction of the canyon pathways was achieved by creating an "Empty 3D cube" on Petrel that allowed the correlation of the mapped horizons in a pseudo-3D approach. Although this approach helped to reduce uncertainties in the correlation of erosional features across different seismic lines, alternative interpretations are still possible, given the wide spacing of the control lines (30-50 km between N-S seismic lines, 25-30 km between W-E seismic lines). These uncertainties may affect the pathway of the canyons that were reconstructed for each horizon, but not their number nor the regional changes visible in the different horizons, thus not affecting our interpretations and conclusions.

4. RESULTS

Seismic interpretation results are presented for four seismic profiles: three oriented N-S and named L1 to L3 from proximal to distal (Fig. 4), and one oriented W-E and named L4 (Fig. 9). L1, L2, and L3 intersect the slope at ca. 1000 m, 1500 m, and 2000 m water depth, respectively, while L4 crosses the slope in between the two islands.

For each horizon, surface and thickness maps have been created to visualize the pathways of the canyons and the distribution of sediment depocenters (Figs. 6 and 7). Fault interpretations have been also performed for all the four profiles (L1 to L3 in Fig. 8, L4 in Fig. 9).

4.1. Seismic facies and their interpretation

The first seismic facies (SF1) is characterized by high to low amplitude, mostly parallel, continuous seismic reflections (Fig. 3). SF1 has been interpreted to represent deep marine fine-grained pelagic sediments (Stow and Piper, 1984; Thiéblemont et al., 2020). Seismic facies SF2 is mainly characterized by high to medium amplitude seismic reflections that are continuous and consistently dipping reflections that create wedge-shaped units away from the axis of the u-shaped erosional features (i.e., channels). This facies is identified as channel levee sediment deposits (Mayall et al., 2006; Janocko et al., 2013). Seismic facies SF3 is mainly chaotic, and when reflections are visible, they are discontinuous to wavy and/or contorted, with variable amplitude, from high to transparent-low (Fig. 3). We interpreted this seismic facies to represent mass-transport deposits (MTDs), such as blocky submarine landslides or large-scale debris flow deposits (Frey Martinez et al., 2005; Bull et al., 2009; Maselli and Kneller, 2018). Seismic facies SF4, which is characterized by variable amplitude, continuous to discontinuous, wavy to sub-parallel reflections, is mainly present within erosional features (Fig. 3) and thus interpreted to represent channel-fill deposit (Mayall et al., 2006). The last seismic facies (SF5) is characterized by moderate-low amplitude, semi-continuous, mounded to wavy reflections which are interpreted to be associated with bottom current deposits, such as contourite drifts and sediment waves (Rebesco et al., 2014).

4.2. Slope canyon-channel systems: seismic stratigraphy, surface and thickness maps

4.2.1. Unit U1 and horizon M2

Unit U1 is confined between horizons M2 and M2a (Fig. 4). It is characterized by parallel to wavy reflection packages that change laterally low to high-medium amplitude and continuous or semi-

continuous reflections (seismic facies SF1, Fig. 3). A few canyon incisions about 2 km wide and 75 to 375 m deep, with facies SF3 and SF4 infill, can be seen on seismic lines L1, L2, and L3 (black arrows in Fig. 4; Fig. 5). Corrected sediment flux for the unit U1 is 1337 km^3/Myr (Table 1).

Horizon M2 is characterized by a high-to-medium seismic reflection amplitude and marks a net change in seismic facies from an overall high-amplitude sequence below M2 to a lower amplitude sequence above, which starts with unit U1. The surface map of horizon M2 shows a gentle slope with a topographic depression between Pemba and Zanzibar islands (Fig. 6A), with deepest part on the southern end of the latter. This depression is also visible in the southern portion of seismic line L1 (Fig. 4). The surface map of horizon M2 (Fig. 6A) and the thickness map of U1 (Fig. 7A) show about ten W-E oriented incisions located along the seismic line L2, that appear less evident where seismic line L1 is located. Larger channels, still oriented W-E, are visible in deeper waters, with three channels that probably feed the area subsequently occupied by the larger canyons C1 and C2 (Figs. 6A and 7A). The truncation of the seismic line L3 below the M2 horizon does not exclude the possibility that large canyons preexisted before the Oligocene. Four additional channels can be observed on the east side of the structural high (H, Figs. 6A and 7A), which represents a permanent feature through time. Unit 1 thickness map shows high thickness values on the northern flank of the canyon C1 (depocenter d1, Fig. 7A) and towards the western side of the map (depocenter d2, Fig. 7A), which corresponds to the topographic depression described before.

4.2.2. Unit U2 and horizon M2a

Unit U2 is bounded by horizon M2a at its base and horizon M3 at its top (Fig. 4). U2 is characterized by medium frequency parallel continuous seismic reflections, mostly with low to medium amplitude (seismic facies SF1, Fig. 3). High to medium amplitude, hummocky to discontinuous and chaotic reflections (seismic facies SF3, Fig. 3) are present in the infill of u- and v-shaped erosional features. Sediment flux for unit U2, corrected for compaction, is 2144 km^3/Myr (Table 1).

Horizon M2a is a hard kick characterized by continuous low to medium seismic amplitude reflections, characterized by multiple erosional features, about 4 km wide and from 75 m to 600 m deep. In the northern and southern portions of seismic line L2 (Figs. 4 and 5), the M2a surface is cut by incisions that are less than 1 km wide and up to 150 m deep. The channels are larger, up to 2 km wide, in the middle of the seismic section (Figs. 4 and 5). In the seismic line L3 (Fig. 4), canyon C1 (about 20 km wide and 600 m deep) and canyon C2 (8 km wide and 675 m deep) are fed by smaller channels visible along line L2 (Fig. 4 and 5). These two canyons are visible along the entire stratigraphic section, up to the modern seafloor. Moving from N to S along seismic lines L1 and L2 (Figs. 6B and 7B), the number of channels, mostly W-E oriented, increases from two to four in the northern portion of the map and from five to twelve in the middle portion. A sinuous erosional feature (S), which is visible in the map of Figures 6B and 7B, appears to follow a preexisting incision, but it is also characterized by a new tributary from NW, where a topographic high (H) is present. This H separates the northern canyon C1 from the southern canyon C2, where the sinuous feature and five channels converge (Figs. 6B and 7B). Its eastern side is characterized by four small incisions (Figs. 6B and 7B).

The thickness of unit U2 is overall higher than unit U1 (Fig. 7B), with two large depocenters corresponding to canyons C1 and C2, and a smaller one (d3) on the eastern flank of the high (Fig. 7B).

4.2.3. Unit U3 and horizon M3

Unit U3 is confined between horizons M3 and M3a at its base and top, respectively (Fig. 4). It is characterized by two seismic facies: (1) medium frequency, continuous and mostly parallel reflections, with low to medium seismic amplitude (seismic facies SF1, Fig. 3) and (2) high to transparent amplitude, discontinuous/chaotic reflections which can be observed mainly within channel incisions (seismic facies SF3, Fig. 3). Reflections of this unit appear locally truncated by the M3a surface at its top. Corrected sediment flux for the unit U3 is 3009 km^3/Myr (Table 1).

Horizon M3 is a continuous hard kick, medium to low amplitude reflection, and it appears concordant with the underlying reflections. The horizon is cut by about thirty-four incisions that are about 1 to 8 km wide (Table 1; Figs. 4 and 5). Changes of seismic facies within the infill of the channels and truncated reflections were used to recognize different episodes of incisions (Fig. 5, L2-C and L2-D). In the seismic line L2 (Fig. 4), the channels are smaller to the north than to the middle or south of the seismic line. In the seismic line L3, the canyons C1 and C2 have a reduced depth when compared with the canyons at the time of M2a. The northern canyon C1 is about 20 km wide and 375 m deep, while the southern canyon C2 is about 8 km wide and 450 m deep (seismic line L3, Fig. 4).

Horizon M3 shows a higher number of incisions compared to horizon M2a (seismic line L2, Fig. 4; central-north and south portions of Figs. 6C and 7C). Small to medium channels are visible from N to S in the seismic lines L1 and L2. Seven incisions from W-NW converge into canyon C1, while six channels converge into C2 (Figs. 6C and 7C). In the southern part of the surface map, three incisions continue to the E without converging into the canyon (Figs. 6C and 7C). The sinuous erosional feature (S) oriented mostly W-E that goes into canyon C2 is also characterized by few tributaries from the north and from the south. The structural high (H, Figs. 6C and 7C) is characterized by four small incisions on the eastern flank, as visible in the seismic line L3 (Fig. 4).

Unit U3 exhibits an overall decrease in thickness from W to E across the study area (Fig. 7C), with just few depocenters on the eastern side. High thickness values can be noted mostly along the seismic line L1 and on the southern portion of the seismic line L2 (Fig. 7C). On the seismic line L3 (Fig. 7C), higher thickness values are visible at the locations of canyons C1 and C2. Sediment depocenters are visible moving east from canyon C1 (d4, Fig. 7C) and in the NW corner of the map (d5, Fig. 7C).

4.2.4. Unit U4 and horizon M3a

Unit U4 lies between horizons M3a at its base and M4 at its top (Fig. 4). The unit is characterized by two seismic facies: parallel, continuous, and medium amplitude reflections (seismic facies SF1, Fig. 3) and medium amplitude continuous but wavy reflections (seismic facies, SF5, Fig. 3). The infill of the channels exhibits two other seismic facies: (1) low to medium-frequency, continuous or semi-continuous reflections, with high to low seismic amplitude (seismic facies SF4, Fig. 3); (2) high amplitude, chaotic, highly discontinuous, and low frequency reflections (seismic facies SF3, Fig. 3). Corrected sediment flux for the unit U4 is 1778 km^3/Myr (Table 1).

Horizon M3a is a hard kick identified by a continuous parallel reflection, which changes from high amplitude to low amplitude moving towards deeper waters (Figs. 4 and 5). M3a can be traced across most of the study area, but in the farthest outboard section the horizon is truncated by the upper horizon M4 at the location of canyon C1(seismic line L3 in Fig. 4; Fig. 5, L3-F). Horizon M3a is cut by a series of channels, between 1 and 7 km wide and 75 to 150 m deep (Figs. 4 and 5). The largest and deepest channels are observed in the middle of seismic lines L2 and L3 (Figs. 4 and 5, L2-D).

Horizon M3a (upper Miocene, Fig. 6D) and the thickness map of Unit 4 show a reduced number of v-shaped incisions W-E oriented, compared to M3. In particular, the number of channels visible offshore Pemba Island is less if compared with the number of channels observed in the previous unit U3 (Table 1), while offshore Zanzibar the number of channels remains constant (Figs. 6D and 7D). Moving from south to north, five channels from W-NW converge as tributaries into canyon C2, following pre-existing erosional features (Figs. 6D and 7D). Thirteen channels converge into canyon C1, as it can be observed in the northern part of the map (Figs. 6D and 7D). The structural high (H, Fig. 6D) is also incised by four small channels on its eastern flank (Figs. 6D and 7D).

Unit U4 highlights a large depocenter in the SW area of the map (Fig. 7D). Reduced sediment thickness characterizes the NW part of the map compared to the underlying Unit U3, while a small depocenter is visible in the NE portion (d6, Fig. 7D).

4.2.5. Unit U5 and horizon M4

Unit U5, confined between horizon M4 and the seabed (Fig. 4), is characterized by four seismic facies: (1) low to medium amplitude, wavy and mostly continuous and medium frequency reflections, in continuity with the unit below (seismic facies SF1, Fig. 3); (2) high amplitude semi-continuous reflections (seismic facies SF4, Fig. 3); (3) chaotic to discontinuous reflections (seismic facies SF3, Fig. 3), interrupted laterally by (4) high amplitude, wavy to hummocky and continuous to discontinuous, reflections (seismic facies SF5, Fig. 3). Sediment flux for unit U5, corrected for compaction, is 1390 km^3/Myr (Table 1).

Horizon M4 is characterized by a hard kick, mostly continuous with medium to high amplitude. A clear decrease in channelization can be noted moving northward in the seismic lines L2 and L3 (Fig. 4 and Fig. 5). In the northern and southern parts of the seismic line L2, the few visible incisions are about 1-2 km wide and less than 75 m deep, while in the central portion of the line they are about 6-10 km wide and about 300 m of deep. In the seismic line L3, the incisions reach a maximum width of 20 km and depth of 300 m (Fig. 5 L3-F). Horizon M4 shows eight channels oriented mostly W-E and converging into the canyon C1 (Figs. 6E and 7E). Five channels, including the sinuous erosional feature (S), feed the canyon C2 (Figs. 6E and 7E). Only three incisions are observed in the eastern side of the structural high (H, Figs. 6E and 7E).

The thickness map U5 shows value increasing trending diagonally from SW to NE, with the highest thickness in the northern part of the map (Fig. 7E). Small incisions are visible along seismic lines L2 and L3, and two depocenters are observed in correspondence of C1 and C2 (Fig. 7E).

The seabed horizon is represented by a hard kick, with high seismic amplitude and continuous reflectivity. The seafloor (Figs. 6F and 7F) shows five channels converging into the canyon C1, while the sinuous erosional feature and two other channels converge into the canyon C2 (Figs. 6F and 7F). In the southern part of the map only one W-E oriented channel does not converge into the C2 (Figs. 6F and 7F).

The total sediment thickness (M2-seafloor, Fig. 7F) highlights a relatively uniform thickness distribution, with higher values associated with sediment depocenter d7 (Fig. 7F), and canyons C1 and C2, and are also visible on the eastern flank of the structural high (H) and along the sinuous erosional feature (S, fig. 7F). Areas with reduced sediment thickness are visible along the northern portion of line L1, on both flanks of canyon C1, and in the NE corner of the map (Fig. 7F).

4.3. Fault distribution and timing: N-S and W-E views of the margin structures

Normal faults are widespread in the study area, and three extensional domains have been distinguished (Figs. 8 and 9). The first fault domain (Group 1) is characterized by normal faults (dip ~50°) that detach in pre-Oligocene units and do not offset the M2 horizon (Figs. 8 and 9). The second domain (Group 2) contains normal faults (dip ~45-50°), detaching pre-Oligocene units and truncating horizon M2 and units above (Figs. 8 and 9). In some cases, the faults reach the seafloor, creating a visible offset, which is indicative of recent tectonic activity. The third extensional domain (Group 3) included all normal faults above the M2 horizon, also cutting the seafloor (Figs. 8 and 9). Faults are more numerous in the upper slope than in the deeper parts of the basin (seismic line L1 Fig. 8 and line L4 Fig. 9). On the western side of the seismic line L4 (Fig. 9), the mapped horizons are strongly dissected by numerous normal faults forming a deep trough, already identified on the surface and thickness maps (Figs. 6 and 7). Seismic reflections in onlap within units U1, U2, and U3, and the presence of growth strata may indicate syn-tectonic deposition of these units (western side of line L4, Fig. 9A). However, because the dataset, including seismic line L4, is cut below horizon M2, we cannot exclude that the displacement of the high angle normal faults started before the Oligocene. Syn-fault deposits are less evident for unit U4 and U5 (Fig. 9A). Furthermore, the thickness of unit U5 in seismic line L4 is affected by the presence of a mass-transport deposit, which prevents us to quantify if syn-tectonic deposition occurred (Fig. 9A-a). All the faults on the west side of the seismic line L4 dip to the west and cut the seafloor (Fig. 9B). About 15 km eastward from the starting point of the seismic line, there are both east and west dipping faults

forming horsts, grabens, and half-grabens (Fig. 9A-b). The deformation generated by these faults changes the dip of the reflectors from W-dipping to E-dipping, forming an anticline (Fig. 9). As visible moving eastward on the seismic section, fault density decreases and the faults are dominantly E-dipping (Fig. 9B).

The timing of the deformation has been evaluated for each group, observing the relationships between mapped horizons and faults domains. Group 1 fault activity started in the Eocene-Oligocene, and we interpret the Base Miocene M2 horizon to mark the cessation of this tectonic phase. Furthermore, in the N-S seismic lines there is no evidence of syn-tectonic deposits that would indicate an alternative timing (Figs. 8 and 9B). Faults in Group 2 offset the M2 horizon (Figs. 8 and 9B), therefore, they are younger than the faults in the first group. Consequently, we consider the onset of Group 2 fault activity to begin during the upper Oligocene-lower Miocene. Furthermore, some of Group 2 faults cut the seafloor, thus indicating that the tectonic activity has been ongoing from Oligocene until recent times. Faults in Group 3 include every fault that detach in units above the M2, thus the tectonic activity of this group postdates the lower Miocene (Figs. 8 and 9B). Some of Group 3 faults also offset the seafloor, indicating that the tectonic activity is still ongoing (Figs. 8 and 9).

5. DISCUSSION

5.1. Evolution of the deep-water drainage network and constraints on the timing of the uplift of Pemba and Zanzibar islands

The formation of the Zanzibar and Pemba islands has long attracted the interest of the scientific community studying the Tanzania margin and the tectonics of the EARS. These islands are unusual for a passive margin setting, which should be characterized by thermal subsidence and thus have no tectonic forces to explain uplift of these anticlines above sea level (Sii and Underhill, 2015). In this study, we reconstructed the evolution of the deep-water drainage network to provide new insights on the formation of the two islands.

On seismic data (Figs. 4 and 5), we observed that several erosional features, including canyons C1 and C2, originated at horizon M2a and cut into horizon M2, completely removing unit U1 in some areas (seismic line L3, Figs. 4, 5 and 7a). The chronological constraints available indicate that the inception of canyons C1 and C2 dates back to about 23 Ma, age of M2a horizon (Fig. 4). Submarine channels became more numerous from horizons M2a to M3, in combination with an increase in sediment flux from 1337 to 3009 km^3/Myr (units U1 to U3, Table 1 and Fig. 2B). A similar trend in sediment flux has been obtained by Said et al. (2015) (Fig. 2B). At that time, coincident with the middle-Miocene Climatic Optimum (MMCO, Mudelsee et al., 2015), East Africa was subjected to strong annual monsoonal cycles (Said et al., 2015) which accentuated the denudation of uplifted regions on land and increased sediment supply to the western Indian Ocean, thus explaining the progradation of deep-water channel system.

Moving upward through the sequence, a reorganization of the deep-water drainage network is observed offshore Pemba Island where seismic lines show a decrease in the number of the channels starting at horizon M3a (~11.5 Ma; Figs. 4, 6D and 7D). At the same time, offshore Zanzibar Island the channels continue to be numerous and active, as suggested by the aggradational stacking pattern. At horizon M4 (5.3 Ma), a significant reduction in the number of channels can be noted also offshore Zanzibar Island in the southward end of the seismic lines (Figs. 4, 6E and 7E). We interpreted this variation as an effect of the uplift of the islands, with Pemba forming first, as evidenced by the decrease in channelization in the middle-upper Miocene, and Zanzibar forming later, during the upper Miocene to lower Pliocene.

Tectonic uplift of the islands is not the only process that may be responsible for the disappearance of deep-water channels along the Tanzania margin: a reduction in sediment supply due to climate, modifications in the drainage network on the continent, and/or sea level fluctuations could have generated similar results. After 15 Ma, the MMCO was followed by a glaciation and a global sea fall (Mudelsee et al., 2015; Miller et al., 2020), and by an accentuated Indian Ocean monsoon at ~7 Ma (Prell and Niitsuma, 1989; Quade et al., 1989), which would have promoted an increase of

sediment supply to the basin and channel development (Posamentier and Allen, 1999). Instead, the channels offshore Pemba Island disappeared at around the same time of horizon M3a (Fig. 4, 6D and 7D). Consequently, it is reasonable to infer that global sea level change and climate are not the primary drivers influencing the reduction of slope channels offshore Pemba, lending support to our interpretation.

The disappearance of the channels offshore Zanzibar Island during the upper Miocene to Pliocene age corresponds to the sea level highstand of the Pliocene Climatic Optimum (Miller et al., 2020). Furthermore, during the Plio-Pleistocene, East Africa underwent an aridification (Cane and Molnar, 2001; Haug et al., 2001) which Said et al. (2015) interpreted to be the cause of the decrease of the sediment supply. Consequently, constraining the main factor controlling channel abandonment offshore Zanzibar Island is more difficult as tectonics, sea level, or climate could have been responsible for the reduction of sediment supply to the basin and thus slope channels.

The influence of sea level changes during the upper Pleistocene and Holocene is different for the two islands and better constrained. While Pemba remained an island during the last sea level lowstand (~20 ka) because the trough separating Pemba from the mainland to the west and from Zanzibar to the south reached ca. 200 m water depth, Zanzibar was connected to the mainland until the beginning of the Holocene (Prendergast et al., 2016). Post-glacial sea level rise and vertical tectonic movements allowed the isolation of Zanzibar during the Holocene (Kourampas et al., 2015). Sediments sourced by the Ruvu River have infilled almost completely the Zanzibar trough, widening the continental shelf in this area (Figs. 1 and 10D).

5.2. Tectonic and paleogeographic reconstructions

Many authors have proposed that the islands of Pemba and Zanzibar, and associated troughs, represent an expression of the EARS (von Staff, 1914; Stockley, 1928 and1942; Moreau and Pakenham, 1940 and 1941, Kent et al., 1971; Sii and Underhill, 2015), nevertheless the tectonic drivers leading to their formation are still a matter of debate. The most recent model was proposed

by Sii and Underhill (2015; see line drawing in Figure 1C). They suggested that the folds leading to the emergence of the islands were created by punctuated contractional deformations associated with the tectonic inversion of pre-existing buried normal fault during the lower Oligocene to upper Miocene, which is coeval with the EARS tectonics. The authors also assumed that the DFZ acted as a buttress for the contractional deformation, inducing uplift of the islands with the original normal faults remaining in net extension. However, more recent studies conducted on free-gravity anomaly data, and deep seismic reflection and refraction data demonstrated the absence of the DFZ offshore northern Tanzania and Kenya (Franke et al., 2015; Klimke and Franke, 2016; Sauter et al., 2018; Vormann and Jokat, 2021).

By integrating the initial observations from Sii et al. (2015) and Sii and Underhill (2015) with the new results of this study, we propose that the two islands are horsts bordered by antithetic and synthetic normal faults (Fig. 1C). These faults generated the footwall uplift forming the islands of Pemba and Zanzibar during the middle-upper Miocene and upper Miocene – lower Pliocene, respectively, and dissect the seafloor, testifying recent tectonic activity (Figs. 8 and 9). A regional stratigraphic section across Pemba trough into Pemba Island (Fig. 10E, Parson et al., 2013, published in Davidson and Steel, 2018) indeed indicates that the island is an antiform dissected by a west-dipping normal fault bounding the trough. Furthermore, gravity anomalies parallel to the western margin of Pemba and Zanzibar islands indicate that the two troughs have a similar structure (Sandwell et al., 2014; Sinha et al., 2019). The extensional regime started in the lower Miocene and is still ongoing, as indicated by the lack of reverse faults dissecting post-Miocene deposits (Figs. 1C, 8 and 9B), the occurrence of surface cutting normal faults (Figs. 8 and 9B), and moment tensors of offshore earthquakes (Fig. 1A; Yang and Chen, 2010). This extensional regime post-dates a phase characterized by tectonic inversion of Mesozoic-aged rift fault that can be traced back to at least the lower Oligocene, as suggested by Sii and Underhill (2015). This inversion was responsible for the initial uplift of the islands but not their exposure above the sea level. The subaerial exposure of the island was instead driven by footwall uplift and likely related to the East African rift

extension, as suggested by previous studies (Kent et al., 1971; Franke et al., 2015; Davidson and Steel, 2018). Rift-related normal faults have dissected the anticline of Pemba, thus explaining westward dips of the bedding in both the hanging wall and footwall of the W-dipping normal fault bordering the Pemba trough. We do not exclude that the structures developed during the Cenozoic are super-imposed on older faults formed during the Karoo rift, as suggested by the similar orientation between the Pemba trough and the Selous Basin (Yemane et al., 2002, and reference therein). Still, a full understanding of the drivers of the pre-Oligocene tectonic inversion and of the geodynamic processes leading to the formation of the Neogene structures is beyond the scope of this paper, also because of the lack of seismic data imaging the deeper stratigraphic intervals.

In Figure 10, we present a paleogeographic model of the region from pre-Oligocene to recent times that includes the development of the two islands with related tectonic structures and the evolution of the slope canyons. The formation of large anticlines (Figs. 1C, 9) likely pre-dates the deposition of M2 and may record the first modification of seafloor topography related to the tectonic inversion (Figs. 10A, 11 – tectonic event T1). We interpreted this first inversion-related uplift to deform the seafloor topography, with minor influence on channels' development. The extensional deformation started in the lower Miocene (Fig. 11 – tectonic event T2) which is clearly testified by fault groups 2 and 3 (Figs. 8 and 9B), syn-depositional faulting (Fig. 9A), and reflection terminations in units U1, U2 and U3 (Figs. 4 and 5 and 9A). This extensional stage promoted the asynchronous exposure above the sea level of Pemba (Figs. 10B, 11 – tectonic event T3) and Zanzibar (Figs. 10C, 11 – tectonic event T4) islands, and the formation of the grabens, affecting the deep-water depositional system. Pemba and Zanzibar troughs acted as a major sink for sediments supplied from the mainland, inducing the disappearance of slope channels since the middle-upper Miocene (Figs. 4, 7D-E, 10B, C and 11). The tectonic processes that have generated the uplift of the islands also contributed to the formation of the two large canyons C1 and C2 (Figs. 4, 6B, 7B, 10D and 11). Canyon C1 has a width of c. 30 km and depth of c. 500 m at >2,200 m water depth and represents the main conduit of sediments for this sector of the western Indian Ocean during the last 20 Myr.

6. CONCLUSIONS

We used seismic reflection data and exploration wells to investigate changes in the stratigraphic and structural configuration of the northern Tanzania margin, offshore Pemba and Zanzibar islands, to infer a sequence of tectonic events that resulted in the formation of the two islands. Regional correlations of dated seismic horizons, integrated with pseudo-3D reconstructions of deep-water canyon-channel systems through time, indicate a decrease of the slope channels offshore Pemba and Zanzibar islands during the middle-upper Miocene and during the upper Miocene to lower Pliocene, respectively. We interpret that the decrease of channels was primarily driven by the deformation of the seafloor caused by tectonic inversion, which progressively disconnected slope canyons from their feeder systems and ended with the formation of the islands. Given the lack of reverse faults dissecting post-Miocene deposits, we propose that the islands have been uplifted in two different phases. First, Mesozoic-aged rift faults have been reactivated and tectonically inverted until the upper Oligocene forming antiforms, with Zanzibar and Pemba islands at its crest. This resulted in partial uplift of the islands, but not their sub-aerial exposure. Subsequently, an extensional regime started during the lower Miocene probably related to the offshore propagation of the EARS. The pre-Oligocene inverted structures have been dismembered by normal faults, active from the Miocene to present day, which created the Pemba-Zanzibar troughs through footwall uplift that led to the subaerial exposure of the islands. The tectonic processes that influenced the evolution of the margin contributed also to the formation of two large deep-water canyons, C1 and C2, which are the main sediment conduits from the continent to the western Indian Ocean since the lower Miocene.

7. DATA AVAILABILITY

The authors confirm that all relevant data are included in the paper. The seismic data acquired by Lamont-Doherty Geological Observatory during the expedition V3618 are available at

https://www.marine-geo.org/index.php. The bathymetric data presented in this study are from GEBCO - General Bathymetric Chart of the Oceans and are available at https://www.gebco.net. All additional data are available upon reasonable request to the authors.

8. ACKNOWLEDGEMENTS

We are grateful to the Tanzania Petroleum Development Corporation (TPDC), WesternGeco and Schlumberger, Royal Dutch Shell, and Shell Tanzania for giving access to the data and allowing the publication of this work. We would like to thank Schlumberger for providing academic licenses of the seismic interpretation software Petrel and Matthew Corrigan for his continuous support. V.M. acknowledges support by the Natural Sciences and Engineering Research Council of Canada (NSERC) Discovery Grant (RGPIN-2020-04461). John Underhill acknowledges the financial support for research studies undertaken on the East African Margin by Shell and access to seismic data by Western Geco and Ion Geophysical. We also thank Stefano Tavani for his constructive comments. The authors declare to have no conflict of interest.

9. Authors contribution

MDS and VM conceived the study. MDS analyzed the data, wrote the manuscript, and drafted the figures with support from VM, DG, PR, DR, BR. DI, JRU, and DK helped with data interpretation as well as contributions to the editing of the manuscript. All the authors reviewed the final version.

FIGURES

Figure 1. A) Bathymetry of the western Indian Ocean in the offshore northern Tanzania. Black and blue lines are the seismic profiles acquired by WesternGeco and Lamont-Doherty Geological Observatory (expedition V3618), respectively. The violet line marks the location of the 2D seismic reflection profile presented for the first time by Sii et al. (2015), and here named PSDM, which line drawing is shown in figure 1C. The orange square is the area for which structural and thickness

maps have been calculated (Figs. 6 and 7). B) Bathymetric map of the western Indian Ocean showing the location of the main structures. White arrows show the GPS velocity data (ellipses are 95% confidence) and are from Saria et al. (2014). C) PSDM line drawing from Sii et al. (2015).

Figure 2. A) Stratigraphic summary of the wells Well-1, Zanzibar-1, Pemba-5, Simba-1, and DSDP-241. w.d.: water depth; elev.: elevation. B) Sediment fluxes along the Tanzania margin corrected for compaction, using porosity values from DSDP-241 (Table 1; DSDP-241, 1989). The blue line indicates the sediment flux from Said et al. (2015), while the pink line indicates the sediment fluxes calculated in this study. Velocity values were extracted from the Well-1 (Maselli et al., 2020). Age constraints for the mapped horizons (M2 to M4) are from Blow (1969), Schlich et al. (1974) and Maselli et al. (2020). U1 to U5: units classified in this study.

Figure 3. Key seismic facies identified in the study area based on reflection attributes (geometry, internal configuration, amplitude, and continuity) and proposed interpretation for the environment of deposition. MTD: Mass-transport deposit.

Figure 4. Seismic lines L1, L2 and L3, N-S oriented (see location in Fig. 1), showing the five seismic horizons and units investigated in this study (age of the horizons provided in Fig. 2). Black arrows used to indicate the incisions at M2 horizon. Black squares indicate the position of close-up views presented in Figure 5. C1: Canyon 1; C2: Canyon 2. Triangles indicate the intersection with seismic lines L4 and PSDM.

Figure 5. Close-up views of the seismic lines marked in Figure 4 by black squares providing details of the seismic facies.

Figure 6. Surface elevation maps of the horizons with 250 m spacing contours in white. Solid black lines indicate the position of the incisions at the surface while dashed black lines indicate potential channel pathway/position. C1: Canyon 1; C2: Canyon 2; H: Structural high; S: sinuous incision.

Figure 7. A-E) Thickness maps of the different units with position of the incisions (solid black lines) visible on the horizon at the base of each unit. Dashed black lines indicate potential channel pathway/position. F) Total sediment thickness map, with incisions visible at the seafloor and contour lines showing the depth of horizon M2 (Fig. 6A). C1: Canyon 1; C2: Canyon 2; H: Structural high; S: sinuous incision; d1-d7: depocenters.

Figure 8. Seismic lines L1, L2, and L3 showing the classification of the fault groups. Black dashed lines indicate the five seismic horizons. Triangles indicate the intersection with seismic lines L4 and PSDM.

Figure 9. Seismic line L4 with the five seismic horizons and units (A) and the classification of the fault groups (B). Triangles indicate the intersection with seismic line L1, L2, and L3 and the location of the structural high (H). In B, black dashed lines indicate the five seismic horizons, while the black dot line indicates the projection of a portion of the PSDM seismic line (Fig. 1C).

Figure 10. A-D) Conceptual model of the evolution of the study area from pre-Oligocene to present day. E) Line drawing adapted from Parson et al. (2013), published by Davidson and Steel (2018), showing large west-dipping normal fault bounding the west side of Pemba. Position of the line drawing indicated in magenta in Figure 10-D.

Figure 11. Tectono-stratigraphic summary of the study area with mapped horizons and the timing of slope channels development from Zanzibar to Pemba islands, main tectonic events, and formation of the islands. C1: Canyon 1; C2: Canyon 2; s.l.: sea level; ?: uncertain information.

Seismic Unit	Age (Ma)	Basal surface (BS)	Seismic facies (Figs. 3 and 5)	Number of channels (W-E)	Depth BS below seafloor in DSDP Site 241 (m)	Mean porosity (%)	Compacted volume (km^3)	Corrected volume (km^3)	Sediment flux (km^3/Myr)	Corrected sediment flux (km^3/Myr)	Sedimentation rate (m/Myr)	Corrected sedimentation rate (m/Myr)
U5	5.3 - 0	M4	SF1, SF3, SF4 and SF5	17 - 19	148	61	6637	7367	1252	1390	34	37
U4	~11.5 - 5.3	M3a	SF1, SF3, SF4 and SF5	25 - 27	280	58	9671	11035	1560	1778	42	48
U3	15 - ~11.5	M3	SF1, SF2 and SF3	34 - 36	380	53	8349	10530	2528	3009	68	81
U2	~23 - 15	M2a	SF1, SF3 and SF4	28 - 29	455	45	13610	17149	1701	2144	46	58
U1	28 - 23	M2	SF1, SF2, SF3 and SF4	10 - 12	464	46	5315	6684	1063	1337	29	36

Table 1. For each units this table shows a summary of: seismic facies, number of channels, compacted and corrected unit volumes, sediment fluxes and related sediment accumulation rates.

References

Angevine, C.L., Heller, P.L., and Paola, C., 1990. Quantitative Sedimentary Basin Modeling, Educ. Course Notes. AAPG Tulsa, Okla. 32, 247.

Anthony, E.J., Besset, M., Zainescu, F., Goichot, M., 2021. Geomorphology of a tropical river delta under pressure: the Rufiji delta, Tanzania—context, channel connectivity and alongshore morpho-sedimentary and hydrodynamic variability. Geo-Marine Letters 41, 24.

Athy, L.F., 1930a. Density, porosity, and compaction of sedimentary rocks. AAPG Bull 14(1),1-24.

Blow, W.H., 1969. Late Lower Eocene to Recent planktonic foraminiferal biostratigraphy. International Conference Planktonic Microfossils, 1st, Geneva. Proc. 1, 199.

Buitner, S., 2014. How plumes help to break plates. Nature 513, 36-37.

Bull, S., Cartwright, J., Huuse, M., 2009. A review of kinematic indicators from mass-transport compexes using 3D seismic data. Marine and Petroleum Geology 26, 1132-1151.

Burke K., 1996. The African Plate. South Africa Journal Geology 99, 339-409.

Calais, E., Ebinger, C.J., Hartnady, C., Nocquet, J.M. 2006. Kinematics of the East African rift from GPS and earthquake slip vector data. In: Yirgu, G., Ebinger, C.J., Maguire, P.K.H. (Eds.), The Afar Volcanic Province within the East African Rift System. Geological Society Special Publication 259, 9-22.

Cande, S.C., Stegman, D.R., 2017. Indian and African Plate motions driven by the push force of the Reunion plume head. Nature 475, 47-52.

Catuneanu, O., Wopfner, H., Eriksson, G., Cairncross, B., Rubidge, B.S., Smith, R.M.H., Hancox, J., 2005. The Karoo basins of south-central Africa. Journal of African Earth Sciences 43, 211-253.

Davidson, I., Steel, I., 2018. Geology and hydrocarbon potential of the East African continental margin: a review. Petroleum Geoscience 24, 57-91

Deep Sea Drilling Project, 1989. Archive of Core and Site/Hole Data and Photographs from the Deep Sea Drilling Project (DSDP). National Geophysical Data Center, NOAA. *doi:10.7289/V54M92G2*

Ebinger, C.J., Sleep, N., 1998. Cenozoic magmatism throughout East Africa resulting from impact of a single plume. Nature 395, 788-791. https ://doi.org/10.1038/27417

Franke, D., Jokat, W., Ladage, S., Stollhofen, H., Klimke, J., Lutz, R., Mahanjane, E.S., Ehrhard, A., Schreckenberger, B., 2015. The offshore East African Rift System: Structural framework at the toe of a juvenile rift. Tectonics 34, 2086-2104. https://doi.org/10.1002/2015TC003922

Frey Martinez, J., Cartwright, J., James, D., 2006. Frontally confined versus frontally emergent submarine landslides: a 3D seismic characterisation. Marine and Petroleum Geology 23, 585-604.

Haq, B.U., Hardenbol, J., Vail, P.R., 1987. Chronology of fluctuating sea levels since the Triassic. Science 235, 1156-1167.

Heirtzler J.R., Burroughs R.H., 1971. Madagascar's paleoposition: new data from the Mozambique Channel. Science 174, 488-490. https://doi.org/10.1126/science.174.4008.488

Janocko, M., Nemec, W., Warchol, M., 2013. The diversity of deep-water sinuous channel belts and slope valley-fill complexes. Marine and Petroleum Geology 41, 7-34.

Kent, P.E., Hunt, J.A., Johnstone, D.W., 1971. The geology and geophysics of coastal Tanzania. Institute of Geological Sciences Geophysical Paper No. 6, H.M.S.O., London.

Klimke, J., Franke, D., 2016. Gondwana breakup: No evidence for a Davie Fracture Zone offshore northern Mozambique, Tanzania and Kenya. Terra Nova 28, 233-244. https://doi.org/10.1111/ter.12214.

Kourampas, K., 2015. Late Quaternary speleogenesis and landscape evolution in a tropical carbonate island: Pango la Kuumbi (Kuumbi Cave), Zanzibar. International Journal of Speleology 44, 293-314.

Lombo Tombo, S., Dennielou, B., Berné, S., Bassetti, M.A., Toucanne, S., Jorry, S.J., Jouet, G., Fontanier, C., 2015. Sea-level control on turbidite activity in the Rhone canyon and the upper fan during the last Glacial maximum and early deglacial. Sedimentary Geology 323, 148-166.

Macgregor, D., 2015. History of the development of Permian-Cretaceous rifts in East Africa: a series of interpreted maps through time. The Geological Society of London for GSL and EAGE 24, 8-20. https://doi.org/10.1144/petgeo2016-155

Maselli, V., Kneller, B., 2018. Bottom currents, submarine mass failures and halokinesis at the toe of the Sigsbee Escarpment (Gulf of Mexico): Contrasting regimes during lowstand and highstand conditions? Marine Geology 401, 36-65.

Maselli, V., Iacopini, D., Ebinger, C.J., Tewari, S., de Haas, H., Wade, B.S., Pearson, P.N., Francis, M., van Vliet, A., Richards, B., Kroon, D., 2020. Large-scale mass wasting in the western Indian Ocean constrains onset of East African rifting. Nature Communications 11, 3456. https://doi.org/10.1038/s41467-020-17267-5

Maselli, V., Kroon, D., Iacopini, D., Wade, B.S., Pearson, P.N., de Haas, H., 2019. Impact of the East African Rift System on the routing of the deep-water drainage network offshore Tanzania, western Indian Ocean. Basin Research 32, 1-15. https://doi.org/10.111/bre.12398

Métivier, F., Gaudemer, Y., Tapponnier, P., Klein, M., 1999. Mass accumulation rates in Asia during Cenozoic. Geophysics Journal 137, 280-318.

Mitchum, R.M. Jr., Vail, P.R., Sangree, J.B., 1977. Seismic stratigraphy and global changes of sea level, part 6: Seismic stratigraphy interpretation of seismic reflection patterns in depositional sequence. In: Payton, C.E. (ed.). Seismic stratigraphy – applications to hydrocarbon exploration, AAPG Memoir 25, 117-133.

Miller, K.G., Browning, J.V., Schmelz, W.J., Kopp, R.E., Mountain, G.S., Wright, J.D., 2020. Cenozoic sea-level and cryospheric evolution from deep-sea geochemical and continental margin records. Science Advances 6, 1-15.

Moreau R.E., Pakenham R.H.W., 1940. Faunistics and Ages of the East African Islands. Nature 146, 462.

Moreau, R.E., Pakenham R.H.W., 1941. The land vertebrates of Pemba, Zanzibar and Mafia: a zoo-geographical study. Proc. Zool. Soc. London, Series A, 110, parts 3 and 4.

Mougenot, D., Recq, M., Virlogeux, P., Lepvrier, C., 1986. Seaward extension of the East African Rift. Nature 321, 599-603. https://doi.org/10.1038/321599a0

Mudelsee, M., Bickert, T., Lear, C. H., Lohmann, G., 2014. Cenozoic climate changes: A review based on time series analysis of marine benthic δ18O records. Rev. Geophysics 52, 333-374.

Mutti, E., Normark, W.R., 1987. Comparing examples of modern and ancient turbidite systems; problems and concepts. In: Leggett, J.K., Zuffa, G.G. (Eds.), Marine Clastic Sedimentology; Concepts and Case Studies. Graham and Trotman, London, 1-38.

Mayall, M., Jones, E., Casey, M., 2006. Turbidite channel reservoirs e key elements in facies prediction and effective development. Marine and Petroleum Geology 23, 821-841.

Nyagah K., 1994. Stratigraphy, depositional history and environments of deposition of Cretaceous through Tertiary strata in the Lamu Basin, southeast Kenya and implications for reservoirs for hydrocarbon exploration. Sedimentary Geology 96, 43-71.

Parsons, W., McCarthy, A., Nilsen, T., 2013. The coastal exploration potential of the Lower Lamu Basin and Pemba Trough from short and long offset 2D marine seismic and potential fields data. EAPCE '13 Conference, 5-8 February 2013, Tanzania 105.

Pickford, M., 2008. Lower Miocene vertebrate fauna from Pemba Island, Tanzania. South African Journal of Science 104, 231-237.

Posamentier, H.W., Jervey, M.T., Vail, P.R., 1988. Eustatic controls on clastic deposition; I, conceptual framework. In: Wilgus, C.K., Hastings, B.S., Kendall, C.G.St.C., Posamentier, H.W., Ross, C.A., Van Wagoner, J.C. (Eds.), Sea-level Change; an Integrated Approach: SEPM Special Publication 42, 109-124.

Posamentier, H.W., Allen, G.P., 1999. Siliciclastic Sequence Stratigraphy: Concepts and Applications. 7, SEPM, Tulsa.

Prell, W.L., Niitsuma, L., 1989. Introduction, background, and major objectives for ODP Leg 117 (Western Arabian Sea) in search of ancient monsoons. Proceedings of the Ocean Drilling Program, Initial Reports 117: College Station, Texas, Ocean Drilling Program, 5-9.

Prendergast M.E., Rouby H., Punnwong P., Marchant R., Crowther A., Kourampas N., Shipton, C., Walsh, M., Lambeck, K., Boivin, N.L., 2016. Continental Island Formation and the Archaeology of Defaunation on Zanzibar, Eastern Africa. PLoS ONE 11, 1-23.

Quade, J., Cerling, T.E., Bowman, J.R., 1989. Development of Asian monsoon revealed by marked ecological shift during the latest Miocene in the northern Pakistan. Nature 342, 163-166.

Rabinowitz, P., 2005. Multi-Channel Seismic Shot Data from offshore Equatorial East Africa acquired during the R/V Vema expedition V3618 (1980). Interdisciplinary Earth Data Alliance (IEDA). doi:10.1594/IEDA/303732

Rebesco, M., Hernández-Molina, J.F., Van Rooij, D., Wåhlin, A., 2014. Contourites and associated sediments controlled by deep-water circulation processes: State-of-the-art and future Considerations. Marine Geology 352, 111-154.

Reeves C.V., 2018. The development of the East African margin during Jurassic and Lower Cretaceous times: a perspective from global tectonics. Petroleum Geosciences 24, 41-56. https://doi'org/10.1144/petgeo2017-021

Reeves, C.V., de Wit, M.J., 2000. Making ends meet in Gondwana: Retracing the transforms of the Indian Ocean and reconnecting continental shear zones. Terra Nova 12, 272-280. https://doi.org/10.1046/j.1365-3121.2000.00309.x

Roberts, E.M., Stevens, N.J., O'Connor, P., Gottified, P.H.G.M., Gottfried, M.D., Clyde, W.C., Armstrong, R.A., Kemp, A.I.S., Hemming, S., 2012. Initiation of the Western Branch of the East African Rift coeval with the Eastern Branch. Nature Geoscience 5, 289-294. https://doi.org/10.1038/ngeo1432

Said, A., Moder, C., Clark, S., Abdelmalak, M.M., 2015. Sedimentary budgets of the Tanzania coastal basin and implications for uplift history of the East African rift system. Journal of Africa Earth Sciences 111, 288-295. http://doi.org/10.1016/j.afrearsci.2015.08.012

Sandwell, D.T., Müller, R.D., Smith, W.H.F., Garcia, E., Francis, R., 2014. New global marine gravity model from CryoSat-2 and Jason-1 reveals buried tectonic structure. Science 346, 65-67. https://doi.org/10.1126/science.1258213

Sansom, P., 2017. A new stratigraphic model for Tanzania: Insights from deep water exploration. Presented at the Third EAGE Eastern Africa Petroleum Geoscience Forum. Maputo, Mozambique. https://doi.org/10.3997/2214-4609.201702406

Sansom, P., 2018. Hybrid turbidite-contourite systems of the Tanzanian margin. Petroleum Geoscience 24, 258-276. https://doi.org/10.1144/petge o2018-044

Saria, E., Calais, E., Stamps, D.S., Delvaux, D., Hartnady, C.J.H., 2014. Present-day kinematics of the East African Rift. Journal Geophysical Research: Solid Earth 119, 3584-3600.

Sauter, D., Ringenbach, J.C., Cannat, M., Maurin, T., Manatschal, G., McDermott, K.G., 2018. Interplated of oceanicc in the West Somali Basin: Insights from long-offset reflection seismic data. Tectonics 37, 588-603.

Schlich, R., Simpson, E.S.W., Gieskes, J., Girdley, W.A., Leclaire, L., Marshall, B.V., Moore, C., Muller, C., Sigal, J., Valuer, T.L., White, S.M., Zobel, B., 1974. DSDP Site 241, Initial report of the Deep Sea Drilling project. Washington DC, 87-138.

Sepulchre, P., Ramstein, G., Fluteau, F., Schuster, M., Tiercelin, J.J., Brunet, M., 2006. Tectonic uplift and eastern Africa aridification. Science 313, 1419-1423. https://doi.org/10.1126/science.1129158

Sii, P., Underhill, J.R., 2015. Role of punctuated subsidence and structural inversion in creating the East African Spice Islands. 77th EAGE Conference & Exhibition, IFEMA. Madrid, Spain.

Sii, P., Underhill, J.R., Jamieson, R., 2015. Role of Structural Inversion along the East African Passive Continental Margin. EAGE, EA11.

Sinha, S.T., Saha, S., Longacre, M., Basu, S., Jha, R., Mondal, T., 2019. Crustal architecture and nature of continental breakup along a transform margin: New insights from Tanzania Mozambique margin. Tectonics 38, 1273-1291. https://doi.org/10.1029/2018TC005221

Steckler, M.S., Watts, A.B., 1978. Subsidence of the Atlantic-type continental margin off New York. Earth and Planetary Science Letters 41, 1-13.

Stockley, G.M., 1928. Report on the Geology of the Zanzibar Protectorate. Zanzibar, Tanzania.

Stockley, G.M., 1942. The geology of the Zanzibar Protectorate and its relation to the East African mainland. Geological Magazine 79, 233-240.

Stow, D.A.V., Piper, D.J.W., 1984. Deep-water fine-grained sediments: facies models. Geological Society, London, Special Publications 15, 611-646.

Thiéblemont, A., Hernández-Molina, F.J., Ponte, J.P., Robin, C., Guillocheau, F., Cazzola, C., Raisson, F., 2020. Seismic stratigraphic framework and depositional history for Cretaceous and Cenozoic contourite depositional systems of the Mozambique Channel, SW Indian Ocean. Marine Geology 425. https://doi.org/10.1016/j.margeo.2020.106192

Tucholke, B.E., Embley, R.W., 1984. Cenozoic regional erosion of the abyssal sea floor off South Africa. In: Schlee, J.S. (Ed.), Interregional Unconformities and Hydrocarbon Accumulation. AAPG Memoir 36, 145-164.

Vail, P.R., Mitchum, R.M., Thompson, S., 1977a. Seismic stratigraphy and global changes of sea level, Part 4: Global cycles of relative changes of sea level. See Payton 1977, 83-97

Vail, P.R., Todd, R.G., Sangree, J.B., 1977b. Seismic stratigraphy and global changes of sea level, Part 5: Chrono-stratigraphic significance of seismic reflections. See Payton 1977, 99-116.

Veeken, P.C.H., van Moerkerken, B., 2013. 2 - The seismic reflection method and its constraints. Seismic Stratigraphy and Depositional Facies Models. Academic Press 15, 17-104.

von Staff, H., 1914. Wissenschaftliche Ergebnisse der Tendagur-Expedition: 1909-1912, Volume 1, Part 3. Paleontographica/Supplementum Geologisch-Paläontologisches Institut und Museum (Berlin), 1-3-7.

Vormann, M., Jokat, W., 2021. Crustal variability along the rifted shared East African margin: a review. Geo-Marine Letters 41, 19.

Yang, Z., Chen, W.P., 2010. Earthquakes along the East African Rift System: A multiscale, system-wide perspective. Journal of Geophysical Research 115, B12309. https ://doi.org/10.1029/2009JB006779

Conflict of interest

The authors declare to have no conflict of interest.

Highlights

This study provides new constraints on the evolution of the North Tanzanian margin.

Changes in canyon-channel systems were reconstructed from Oligocene to recent times.

Uplift of Pemba and Zanzibar islands controlled the evolution of slope systems.

Pemba and Zanzibar formed during mid-upper Miocene and Mio-Pliocene, respectively.

Extensional regime associated with islands' emersion may be related with the EARS.